Theoretical Study of Boron−Ammonia Reactions

Zhi-Xiang Wang,[†,‡] Ming-Bao Huang,[‡] and Paul von Ragué Schleyer*[,‡]

Graduate School at Beijing, University of Science and Technology of China, Academia Sinica, Beijing 100039, P.R. China, and Center for Computational Quantum Chemistry, University of Georgia, Athens, Georgia 30602

Received: May 11, 1999

The mechanisms of the reactions of a boron atom (^{2}P) and of B_2 ($^3\Sigma_g^-$) with ammonia were studied computationally at the hybrid DFT B3LYP/6-311++G(3df, 2p)//B3LYP/6-311++G(2d,p) level. The B and B_2 insertions into NH bonds take place by initial formation of BNH_3 and $BBNH_3$ complexes. As found previously for methane and water, B_2 also is more reactive than B with ammonia. The energy-rich boron atom insertion product, $HBNH_2$, then gives the species $HBNH_2$, H_2BNH, HBNH, and BNH. These can react with a second boron atom to give novel boron-containing compounds such as HBNBH, BNBH, H_2BNBH, and BNB, some of which have been observed experimentally. However, contrary to the experimental suppositions, the only cyclic B_2N minimum was a high-energy species.

Introduction

The reactions of a boron atom with small molecules, such as CH_4,[1−6] NH_3,[7−10] H_2O,[3,11−12] C_2H_2,[13−16] N_2(N),[17−19] CO_2,[20] CO,[21,22] O_2,[23] and H_2,[24] have been investigated extensively. Many of the novel boron-containing products characterized computationally also have been observed experimentally. Andrews and co-workers reacted boron atoms, generated by laser ablation, with NH_3 under matrix isolation conditions.[7,8] The initial step was proposed to involve the insertion of B into NH_3 to form the $HBNH_2$ complex; several reaction channels then were followed to generate HBNH, BNH, H_2BNH, $HBNH_2$, etc. The reactions of a second boron with these primary species led to species such as HBNBH, HBNB, linear BNB, and, putatively, cyclic-B_2N. The electron spin resonance (ESR) investigation of Knight et al.[9,10] also demonstrated BNH to be one of the products from the boron−ammonia reaction. Being isoelectronic with acetylene, HBNH (iminoborane) has attracted special attention.[25] The reactivity of iminoboranes and their stabilization by substituents has been investigated by Paetzold et al.[26] Although the major species generated[10] in the reaction of B with NH_3 were characterized theoretically in the experimental papers,[7,8] no computational study of the reaction mechanism has been reported.

Several groups have investigated the reactions of B with CH_4, H_2O, and C_2H_2 theoretically. Martin et al.[13] provided computational support for the experimental identification[14] of the borirene radical, BC_2H_2; two other groups[15,16] elucidated the complicated mechanism for the reaction of B with C_2H_2. Our recent B3LYP DFT calculations found B_2 to be more reactive than a single boron atom with methane and water.[4] The calculated activation energies for B insertion into methane and water differed significantly from those previously predicted at the semiempirical or lower ab initio levels.[5]

We have now studied the mechanism of the reactions occurring in the boron−ammonia system in great detail and try to explain the formation of the novel boron-containing compounds identified experimentally. Although the energy of the reacting B atoms generated experimentally is not known,[8] we follow the experimentalists' lead[18] and only consider the reaction of the ^{2}P B-atom ground-state here. The ^{2}S B-atom excited state is 4.96 eV[27] higher in energy. While the laser wavelength used for ablation was 1064 nm (1.17 eV), multiphoton process might be involved. The insertion of ground-state B_2 ($X^3\Sigma_g^-$, which is 3.79 eV[28] lower in energy than the first $A^3\Sigma_u^-$ excited state) also was investigated to see if B_2 also is more reactive than a single boron atom with NH_3.[4]

Computational Methods

As in our previous study[4] of the B and B_2 insertions into CH_4 and H_2O, the hybrid B3LYP DFT method[29] was employed. Using the GAUSSIAN 94 program,[30] stationary points were optimized and characterized by frequency analysis initially at the B3LYP/6-31G(d) level. For transition states, the vibration modes corresponding to the imaginary frequencies were drawn in the Figures 2, 4, 7, and 9 (see below). The geometries, reoptimized with the larger basis sets, 6-311++G(d, p) and 6-311++G(2d, p),[31] were used to refine the energies by performing B3LYP/6-311++G(3df, 2p) single-point calculations. The B3LYP/6-31G(d) zero-point energies (ZPEs), scaled by a factor of 0.9804,[32] were used to correct the relative energies. The minimum-energy paths (MEP) of some of reactions were traced to confirm the connections to the presumed products. The spin contaminations of the B3LYP open-shell calculations were all small, with $\langle S^2 \rangle$ being less than 0.78 for doublet species and 2.15 for triplet species.

To check the reliability of the DFT results, the ab initio G2[33] and CCSD(T)[34] methods were used to reinvestigate the initial reaction step. The CCSD(T) calculations were performed with

[†] University of Science and Technology of China.
[‡] University of Georgia.

10.1021/jp991546e CCC: $18.00
Published on Web 07/16/1999

TABLE 1: Energies[a] (in kcal/mol) for the Initial Reaction ($B + NH_3 \rightarrow$ Products) and the Insertion of B_2 into NH_3, Together with the B3LYP/6-31G(d) Zero-Point Energies (ZPE, in kcal/mol) and Imaginary Frequencies (IMG, in cm^{-1}) for Transition States

		ZPE[b]	IMG	6-31G(d)	6-311++G(d,p)	6-311++G(2d,p)	6-311++G(3df,2p)[d]	G2	CCSD(T)/6-311++G**
$B + NH_3$	**1**	21.3		0.0	0.0	0.0	0.0	0.0	0.0
				(−81.20229)[c]	(−81.24519)	(−81.24656)	(−81.24954)	(−81.06066)	(−81.02692)
$B-NH_3$	**2**	22.5		−12.2	−12.8	−12.9	−13.1	−11.2	−9.2
TS	**2/3**	18.9	1698.3i	−1.0	−1.4	−1.7	−2.2	3.6	6.3
$BHNH_2$	**3**	22.4		−97.8	−93.6	−93.9	−94.4	−88.6	−84.6
TS	**3/4**	17.4	1867.9i	−56.7	−53.3	−54.0	−54.6	−46.3	−41.1
H_2BNH	**4**	18.8		−97.5	−89.8	−90.3	−90.9	−81.9	−77.9
TS	**3/5**	16.4	1018.6i	−62.1	−57.4	−57.9	−58.2	−51.4	−45.6
HBNH + H	5	15.6		−68.0	−63.3	−63.8	−64.3	−61.3	−56.8
TS	**3/6**	17.0	1545.9i	−30.2	−30.0	−30.9	−31.4	−24.5	−19.1
$BNH + H_2$	**6**	15.0		−60.2	−56.2	−56.6	−57.3	−53.7	−50.0
H_2NB+H	**7**	15.4		−23.2	−22.2	−22.7	−23.1	−22.3	−20.0
$NBH+ H_2$	**8**	15.0		−26.7	−18.6	−19.3	−19.7	−16.1	−12.9
$BH + NH_2$	**9**	14.9		19.8	23.3	22.6	22.7	23.6	25.7
$B_2 + NH_3$	**10**	22.8		0.0	0.0	0.0	0.0		
				(−105.96361)	(−106.01001)	(−106.01220)	(−106.01583)		
B_2-NH_3	**11**	26.1		−32.7	−34.2	−34.2	−34.6		
TS	**11/12**	22.4	1628.4i	−16.0	−16.7	−16.6	−17.1		
$NH_2B(B)H$	**12**	24.7		−100.0	−96.4	−96.5	−96.9		

[a] Corrected with the B3LYP/6-31G(d) zero-point energies (scaled by a factor of 0.9804[32]). [b] Scaled zero-point energies. [c] Values in parentheses are the total energies in au. [d] Single-point calculations at the B3LYP/6-311++(2d,p) geometries.

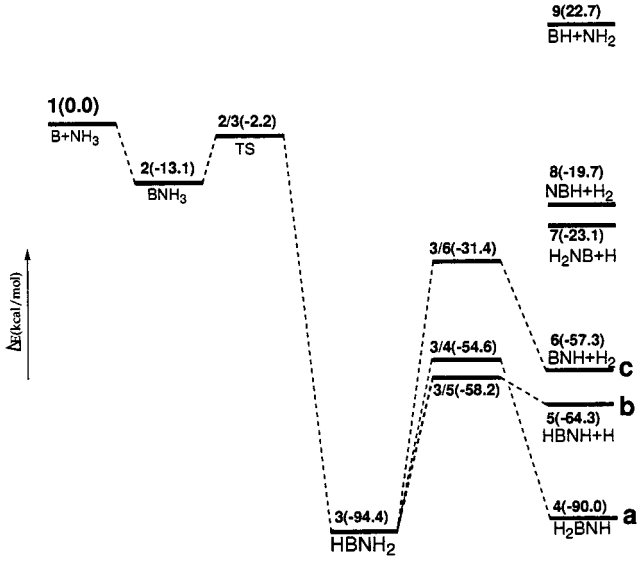

Figure 1. Schematic PES for reaction $B + NH_3 \rightarrow$ products (channels: (a) **3** → **3/4** → **4**; (b) **3** → **3/5** → **5**; (c) **3** → **3/6** → **6**). The values in parantheses are the B3LYP/6-311++G(3df,2p) + ZPE (B3LYP/6-31G(d)) relative energies in kcal/mol.

the 6-311++G** basis set, and the relative energies were corrected with the scaled B3LYP/6-31G* zero-point data (Table 1).

In the following text, we denote the minimum-energy points as **1**, **2**, ... and the transition states connecting, e.g., **1** and **2** as **1/2**. For consistency, the B3LYP/6-311++G(2d,p) geometries and B3LYP/6-311++G(3df, 2p) energies are discussed unless stated otherwise.

Results and Discussion

Initial Reaction of Boron−Ammonia System. The initial step of the reaction of B with NH_3 is predicted to occur along the potential energy surface (PES) shown schematically in Figure 1. The structures of the stationary points in Figure 1, together with key B3LYP/6-311++G(2d, p) geometric parameters, are displayed in Figure 2; the energies calculated at the various levels are compiled in Table 1, along with the scaled zero-point energies (ZPEs) and the imaginary frequency values of transition states.

Insertion of B(^{2}P) into NH_3. Like the insertion of boron into water,[4] an initial complex, $B-NH_3$ (**2**), preceding transition state **2/3** was located along the pathway of B insertion into NH_3 (see the part shown to the left of **3** in Figure 1). The formation of such complexes involves the interaction between the empty p-orbital of B and the heteroatom lone pair(s) of ammonia and water. Methane obviously cannot function in this manner.[4] The mechanisms for B insertion into CH_4, NH_3, or H_2O are similar to that for CH (or SiH) insertion.[35−38] This is reasonable since, effectively, the B atom is isolobal with the C atom, as well as with CH or SiH.

Our calculations predict that **2** and the product $HBNH_2$,(**3**), have C_s symmetry. Our bond lengths for **3** are only slightly shorter than those at the CASSCF/cc-pvdz level,[8] but our 1.701 Å N−B distance in weakly bound **2** is 0.213 Å shorter than that reported in ref 8. Since nitrogen is a better lone-pair donor than oxygen, the binding energy of **2,** 13.1 kcal/mol (to separated B and NH_3), is larger than the binding energy of 5.5 kcal/mol for the $B-OH_2$ complex (computed at the same level). Our previous studies[35−38] of CH and SiH insertions also found the $HCNH_3$ and $HSiNH_3$ donor−acceptor complexes to be more stable than $HCOH_2$ and $HSiOH_2$ complexes. The three-center **2/3** transition state is similar to that for B insertion into methane or water;[4] the N−B, B−H, and N−H distances are 1.522, 1.507 and 1.193 Å, respectively. As the reaction proceeds from **2/3**, the N−B and B−H bonds form, the N−H bond breaks, and the $HBNH_2$ (**3**) insertion product results. The energies of **2**, **2/3**, and **3** relative to **1** are computed to be −13.1, −2.2, and −94.4 kcal/mol, respectively. Thus, the insertion is very favorable energetically, and the **2** → **2/3** barrier is only 10.9 kcal/mol.

The Al atom insertion into ammonia has been studied by Sakai[39] at the MP4/6-31+G(d,p)//HF/6−31(d,p) level. The predicted mechanism is similar to that for B insertion. However, the insertion of B into NH_3 takes place more easily than Al into NH_3. The relative energies (vs Al + NH_3) of the $AlNH_3$ complex, transition state, and product were computed to be

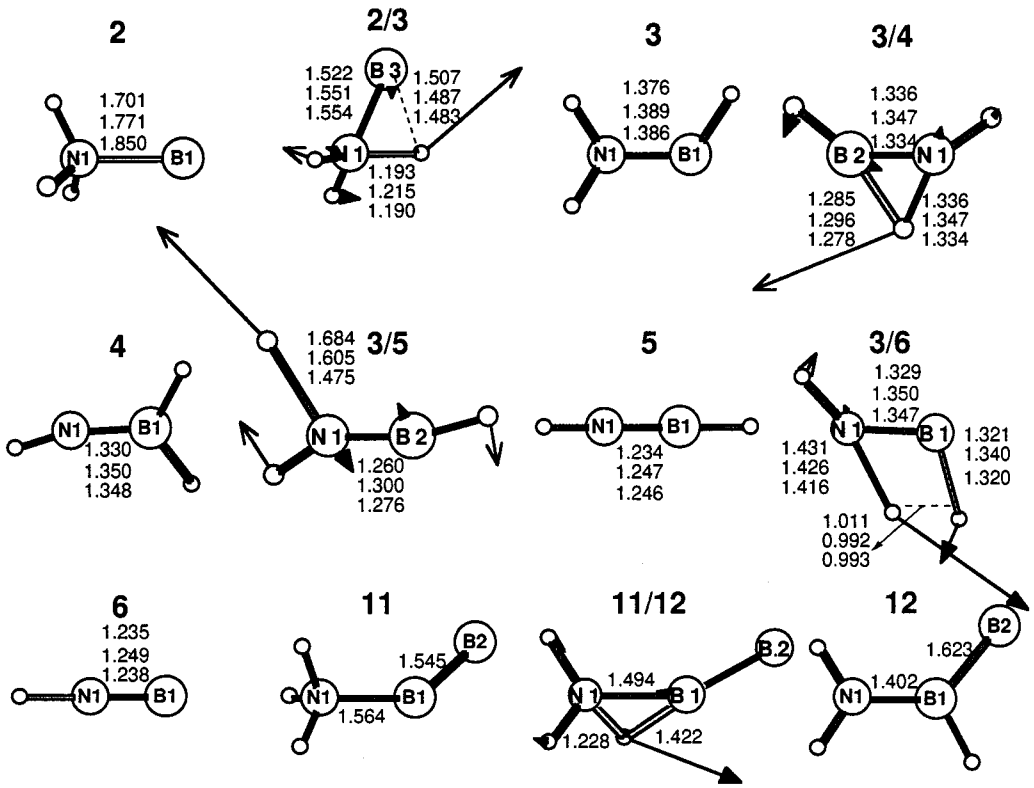

Figure 2. B3LYP/6-311++G (2d,p) structures for the stationary points along the reaction pathways B + NH_3 → products and B_2 + NH_3 → products, including the MP2/6-31G* (middle) and CCSD(T)/6-311++G** (bottom) data. Bond lengths are in Å.

−11.7, 16.0, and −30.4 kcal/mol, respectively, compared to our DFT values (−13.1, −2.2, and −94.4 kcal/mol) for the reaction of B with NH_3.

The alternative process, direct H-abstraction by B leading to BH + NH_2, is endothermic (22.7 kcal/mol). The activation energy for the H-abstraction could be even more unfavorable. However, BH and NH_2 radicals might be formed experimentally if the boron atoms generated from laser ablation are hyperthermal.

Comparison of B and B_2 Insertions into NH_3. The mechanism for B_2 insertion into NH_3 is predicted to be similar to that of B insertion. Structures **11**, **11/12**, and **12** in Figure 2 represent the optimized geometries of the intermediate $BBNH_3$ complex, the transition state for B_2 insertion into NH_3, and the B−BH−NH_2 product. The energies, included in Table 1, show the complex **11** to be much more strongly bound than BNH_3, **2**. Also, the energies of the transition states **11/12** and **2/3,** −17.1 and −2.2 kcal/mol relative to the respective reactants, are quite different. This behavior supports and extends our previous conclusion that the reactivity of B_2 is higher than that of a single B atom in insertion.[4]

Subsequent Reactions Following B Insertion into NH_3. The $HBNH_2$ (**3**) species produced by B insertion into NH_3 possesses 94.4 kcal/mol excess energy; this is close to the 89 ± 2 kcal/mol previously computed at the CCSD(T)/cc-pVTZ level.[8] The energy-rich species **3** can relax (if a third body is present) to give free $HBNH_2$ or can rearrange or dissociate to generate other fragments. As shown in Figure 1 (to the right of **3**), there are six possible reaction channels leading to **4** (H_2BNH), **5** (HBNH + H), **6** (BNH + H_2), **7** (BNH_2), **8** (NBH + H_2), and **9** (BH + NH_2); the relative energies (vs **1**) are −90.9, −64.3, −57.3, −23.1, −19.7, and 22.7 kcal/mol, respectively.

We focus first on the channels leading to **4**, **5**, and **6**. With respect to the reactants **1**, all the three channels (denoted (a), (b), and (c) in Figure 1) are strongly exothermic. Channel b, the most favorable, proceeds via transition state (**3/5**) which is 36.2 kcal/mol above product **3** in energy but 58.2 kcal/mol below **1.** The separation of breaking N−H bond is 1.684 Å in **3/5**. Channel a has not been considered previously, but the activation energy is only 3.6 kcal/mol higher than that for channel b. Channel a involves H-migration via transition state (**3/4**). Channel c proceeds by 1,2-H elimination via a transition state (**3/6**); the barrier height is 63.0 kcal/mol. The length of the forming H−H bond is 1.011 Å in **3/6**, and the bond distances of the breaking N−H and B−H bonds are 1.431 and 1.321 Å, respectively. No transition states were found for the channels leading to **7** and to **9.** The channel leading to **8** requires the breaking of two N−H bonds and, as expected, has a very high energy barrier.

It is interesting to compare these reactions with those involved in the insertion of B into water. The HBO and BO radicals, the primary products of the B + H_2O reaction,[11] are proposed to be formed via H-dissociation and by 1,2-H elimination of HBOH. The two processes are analogous to the channels b and c discussed above, respectively, and have been confirmed in a theoretical study.[12] However, a channel leading to H_2BO, analogous to channel a, has not been considered by experimentalists or theoreticians before.

On the basis of the DFT energies, the species (along with H and H_2) generated in the initial reaction of B with NH_3 are $HBNH_2$, HBNH, BNH, and H_2BNH. All these have been observed experimentally except H_2BNH. However, HB, NH_2, and BNH_2 might also be detectable as minor products if hyperthermal boron atoms from laser ablation are generated.

Comparison with G2 and CCSD(T) Results. G2 and CCSD(T)/6-311++G** calculations were performed to confirm the DFT relative energies for the initial reaction steps (see the comparisons in Table 1). Among the three levels of theory, DFT

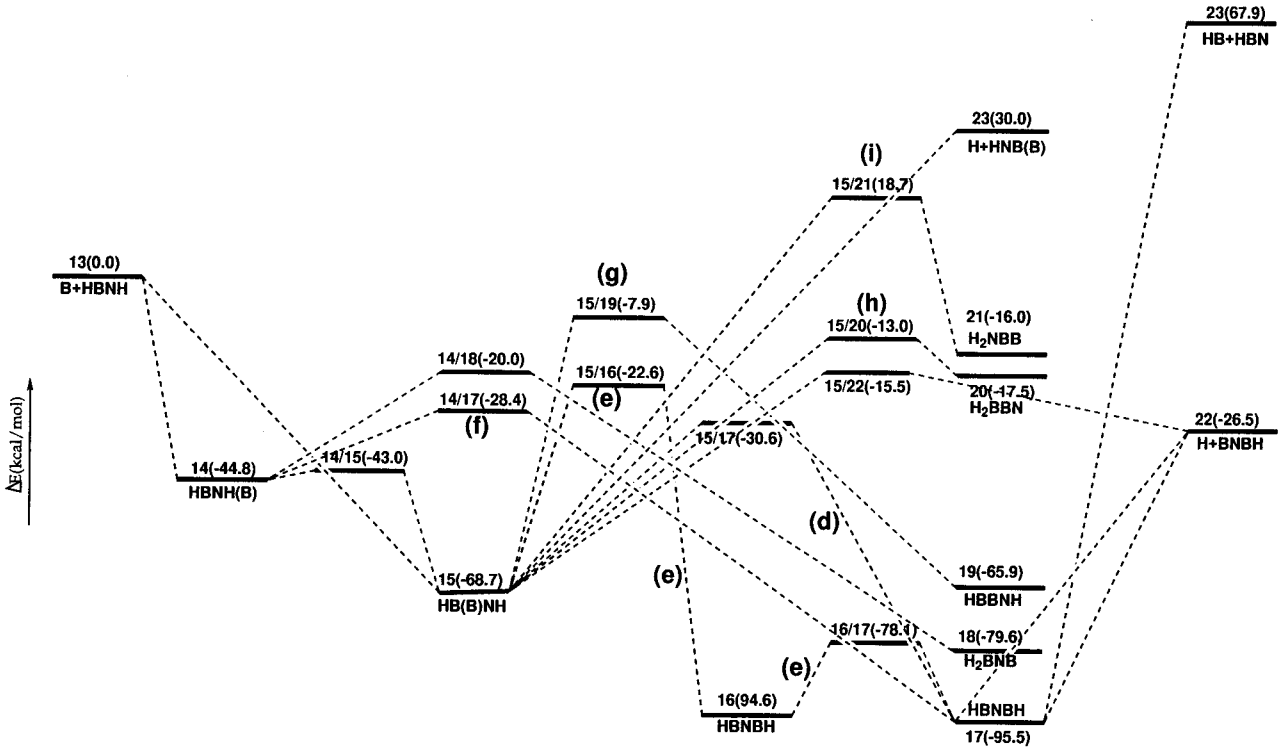

Figure 3. Schematic PES for reaction B + HBNH → products (channels: (d) **15** → **15/17** → **17**; (e) **15** → **15/16** → **16** → **16/17** → **17**; (f) **14** → **14/17** → **17**). The values in parantheses are the B3LYP/6-311++G(3df,2p) + ZPE (B3LYP/6-31G(d)) relative energies in kcal/mol.

TABLE 2: Energies[a] (in kcal/mol) for the Reaction (B + HBNH → Products), Together with the B3LYP/6-31G(d) Zero-Point Energies (ZPE, in kcal/mol) and Imaginary Frequencies (IMG, in cm^{-1}) for Transition States

		ZPE[b]	IMG	6-31G(d)	6-311++G(d,p)	6-311++G(2d,p)	6-311++G(3df,2p)[d]
B + HBNH	**13**	15.6		0.0 (−105.45564)[c]	0.0 (−105.49726)	0.0 (−105.49960)	0.0 (−105.50340)
HBNH(B)	**14**	16.9		−46.4	−43.8	−44.4	−44.8
TS	**14/15**	16.0	691.3i	−44.4	−42.0	−42.5	−43.0
HB(B)NH	**15**	18.2		−72.2	−67.3	−68.1	−68.7
TS	**15/17**	13.3	1498.6i	−32.4	−28.8	−29.7	−30.6
TS	**14/17**	13.2	1511.2i	−30.0	−26.5	−27.5	−28.4
TS	**15/16**	15.2	1278.5i	−26.3	−21.2	−22.1	−22.6
HBNBH	**16**	16.8		−100.8	−93.8	−94.1	−94.6
TS	**16/17**	15.4	699.5i	−83.4	−77.4	−78.0	−78.1
HBNBH	**17**	15.6		−100.9	−94.0	−94.7	−95.5
TS	**14/18**	0.0	1662.5i	−20.2	−18.1	−18.3	−20.0
H_2BNB	**18**	17.0		−86.7	−78.0	−78.9	−79.6
TS	**15/19**	14.5	279.7i	−10.2	−7.6	−7.7	−7.9
HBBNH	**19**	15.9		−67.0	−65.3	−65.2	−65.9
TS	**15/20**	14.3	1237.5i	−17.0	−12.0	−12.7	−13.0
H_2BBN	**20**	16.2		−24.1	−16.9	−17.2	−17.5
TS	**15/21**	15.2	1390.3i	18.3	19.3	18.9	18.7
H_2NBB	**21**	18.0		−15.1	−16.0	−15.7	−16.0
TS	**15/22**	11.5	1126.8i	−18.5	−14.7	−15.5	−15.5
H + BNBH	**22**	10.9		−29.2	−25.0	−25.7	−26.5
HB + HBN	**23**	12.0		64.4	68.2	67.7	67.9
H_2 + BNB	**24**	10.2		−27.9	−23.3	−24.0	−25.0
H + BNB(H)	**25**	10.2		30.7	31.1	30.5	30.0

[a] Corrected with the B3LYP/6-31G(d) zero-point energies (scaled by a factor of 0.9804[32]). [b] Scaled zero-point energies. [c] Values in parentheses are the total energies in au. [d] Single-point calculations at the B3LYP/6-311++(2d,p) geometries.

predicts the lowest relative energies; these are on average 4.6 and 8.4 kcal/mol lower than at G2 and at CCSD(T), respectively. Note that the spin contaminations in the G2 and CCSD(T) calculations for **2/3** are large, $\langle S^2 \rangle$ being about 0.97. More important, the three methods give the same relative energy order for the various species. For example, the energy differences between **3/4** and **3/6** are predicted to be 26.9, 26.5, and 26.8 kcal/mol at the G2, CCSD(T), and DFT levels, respectively, and 21.8, 22.0, and 23.2 kcal/mol between **3/5** and **3/6**. Therefore, the G2 and CCSD(T) energies do not change the conclusions drawn from the DFT results.

The energies relative to separated B and NH_3 for B insertion into NH_3 are predicted to be 3.6 and 6.3 kcal/mol at the G2 and CCSD(T)/6-311++G** levels, respectively, compared with the B3LYP value of −2.2 kcal/mol mentioned above. Taking the experimental conditions into account, the insertion should

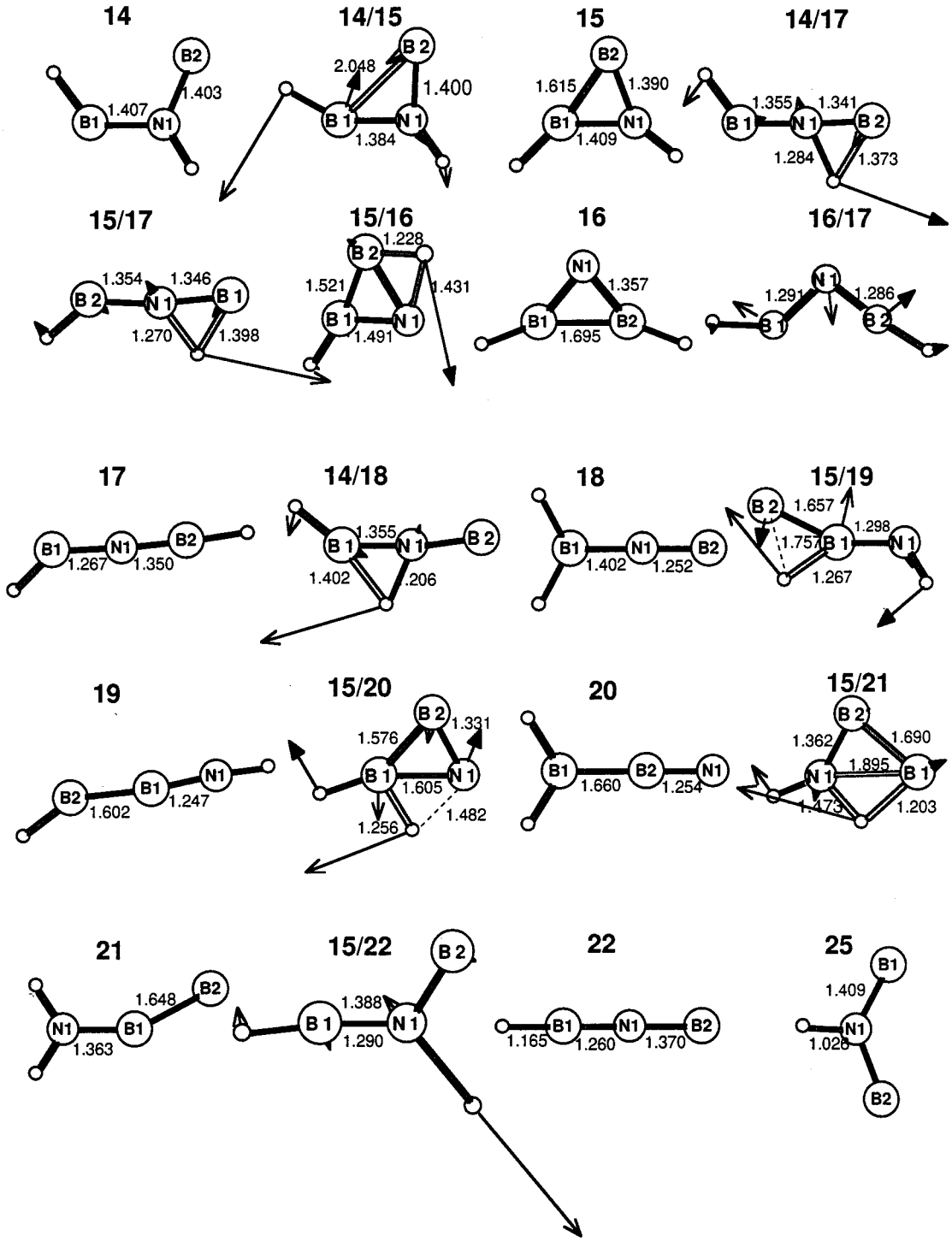

Figure 4. B3LYP/6-311++G(2d,p) structures for the stationary points along the reaction pathway B + HBNH → products. Bond lengths are in Å.

occur easily even with the small activation energies computed at G2 and CCSD(T).

The structural parameters at the G2 and CCSD(T)/6-311++G** levels, also given in Figure 2, are in reasonable agreement with the B3LYP data.

Reactions of a Second B with Major Species Generated in the Initial Step. Besides these initial and minor species, Andrews et al.[7,8] observed other molecules such as HBNBH, BNBH, and BNB and discussed some evidence for "cyclic-B_2N". These species were produced by the reactions of a second B atom with the primary HBNH product. The following section deals with the reaction of a second B with product HBNH, BNH, H_2BNH, and $HBNH_2$.

B + HBNH → Products. Figure 3 shows the schematic PES for the reaction of B with HBNH. Energy data for the various channels are summarized in Table 2 and the structures of the stationary points are shown in Figure 4.

The first step is the addition of B to HBNH. Although five possible structures, A−E, were considered, we could only locate the addition complexes **14** (corresponding to (B)) and **15** (corresponding to (C)) displayed in Figure 5. Flores and Largo[15] showed that the only ring structure of the $B-C_2H_2$ addition

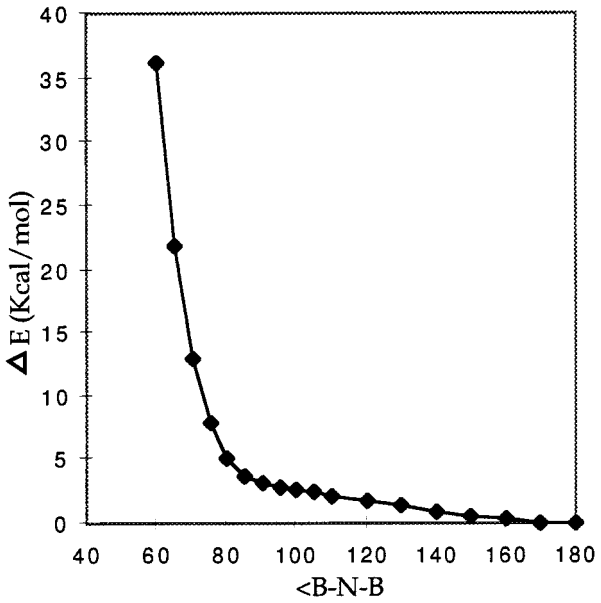

Figure 5. Total energy of BNB as a function of the B−N−B angle at the B3LYP/6-31G(d) level in C_{2v} symmetry.

complex (acetylene is isoelectronic with HBNH) is similar to **15**. The previously reported cis and trans structures of $B-C_2H_2$[16] were UHF artifacts due to the large spin contamination.

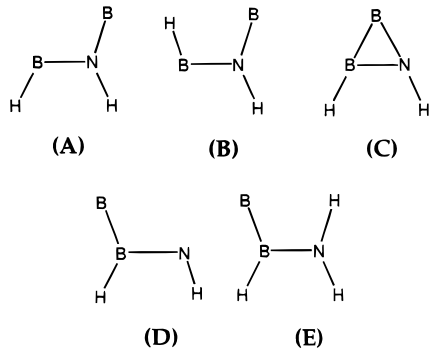

Structures **14** and **15** are predicted to be 44.8 and 68.7 kcal/mol, respectively, lower in energy than the reactants **13** (B + HBNH). The exothermicity of the addition reaction can overcome energies for subsequent reactions. The activation energy for the rearrangement of **14** to **15** via transition state **14/15** is only 1.8 kcal/mol; hence **14** is extremely unstable toward **15**.

Following the additions, three reaction channels give the HBNBH (**17**) species; they are denoted as (d) (**15** → **15/17** → **17**), (e) (**15** → **15/16** → **16** → **16/17** → **17**) and (f) (**14** → **14/17** → **17**) in Figure 3. The activation energies (relative to **15** for (d) and (e) and to **14** for (f)) for the three reactions are computed to be 38.1, 46.1, and 16.4 kcal/mol, respectively. However the transition states **15/17**, **15/16**, **16/17,** and **14/17** are −30.6, −22.6, −78.1, and −28.4 kcal/mol lower in energy than reactants **13**, respectively. The energies indicate that the three reactions are feasible energetically, in agreement with the experimental observation of the HBNBH species.[7] Note that reaction f cannot compete with the rearrangement of **14** to **15** (which has an activation energy of only 1.8 kcal/mol).

Reaction d was confirmed by tracing the MEP starting at the transition state **15/17** in both the forward and reverse directions at the B3LYP/6-31G(d) level. Andrews and co-workers[7,8] suggested a direct insertion mechanism for B into HBNH. Apparently, HBNBH (**17**) (as well as **19**, see below) can be considered to be a product of B insertion into HBNH.

HBNBH (**17**) is 95.5 kcal/mol lower in energy than reactants **13** but might dissociate into **22** (BNBH + H) and **23,** which is 26.5 kcal/mol lower in energy than reactants (**13**). The alternative is unfavorable: **23** (HB + HBN) is 67.9 kcal/mol higher than **13**. No transition state was located for either of the two dissociation channels. A possible channel leading to H_2 + BNB via 1,3-H elimination from **17**, suggested by Andrews and co-workers,[7,8] was not found in the present study. It must be very high in energy since the two H atoms are far away from each other in **17** (see Figure 4). The N−H bond cleavage in **15** via a transition state **15/22** also results in BNBH + H (**22**). The barrier height for this cleavage is predicted to be 53.2 kcal/mol (relative to **15**), which is larger than the (overall) barriers of 38.1 and 46.1kcal/mol for reactions d and e. B−H bond cleavage in **15** is predicted to have no transition state; the energy of the product **25** is 30.0 kcal/mol higher than **13**.

Starting from the addition complex **15**, there are three more reaction channels (see Figure 3) denoted as (g) (**15** → **15/19** → **19**, the insertion of B into the B−H bond of HBNH), (h) (**15** → **15/20** → **20**), and (i) (**15** → **15/21** → **21**). The energies of the transition states for these three reactions are −7.9, −13.0, and 18.7 kcal/mol relative to the reactants (**13**), while the energies of the products (**19**, **20**, and **21)** are −65.9, −17.5, and −16.0 kcal/mol, respectively. Compared with channels d, e, and f, channels g, h, and i may be neglected due to their larger activation energies (see Figure 3 for comparison). While the addition complex **14** can rearrange into H_2BNB (**18**) via transition state **14/18**, this channel also may be neglected, since the barrier (24.8 kcal/mol) is much higher than that (1.8 kcal/mol) for the rearrangement of **14** to **15**.

Is There a Cyclic B_2N Isomer? Andrews and co-workers[7,8] discuss evidence for a cyclic form of B_2N which might have formed from **15** by 1,2-H elimination. We expended considerable effort in searching for this reaction path, without success. To our surprise, we even failed to locate a cyclic-B_2N stationary point on the ground-state PES at correlated levels. We did reproduce the structure reported in ref 19 at (U)HF/6-31G(d), but reoptimization at the B3LYP level gave the linear form with electronic configuration ($X^2\Sigma_u^+$: $3\sigma_g^2 2\sigma_u^2 1\pi_u^4 4\sigma_g^2 3\sigma_u^1$). We scanned the PES of B_2N by performing partial optimizations at fixed B−N−B angles with and without C_{2v} restrictions. The curve given in Figure 5 describes the variation of the total energy with the NBN angle and shows that there is no energy minimum for a bent C_{2v} structure. C_s searches gave the same result. Other post-SCF calculations failed to characterize a cyclic-B_2N.[40] The ESR and CI study of Knight et al.[9,10] also showed B_2N to have a linear ground state.

The isomer of BNB, BBN, also has linear structure with electronic state $X^2\Sigma^+$ ($6\sigma^2 1\pi^4 7\sigma^1$). It is 55.3 kcal/mol higher than BNB. The B−B and B−N bond distances are 1.283 and 1.532 Å, respectively. The activation energy for isomerization from BNB to BBN 56.3 kcal/mol. In the transition state, the B−B and B−N bond distances and N−B−B bond angle are 1.533 Å, 1.575 Å, and 136.4°, respectively. The $\langle S^2 \rangle$ values for BBN and the transition state are 1.05 and 0.86, respectively.

However, when the initial guess was altered, a cyclic-B_2N minimum ($^2A_1$) was located, which has N−B and B−B bond distances of 1.380 and 1.500 Å respectively. It is 40.6 kcal/mol above the linear BNB ground state. The molecular orbitals ($4a_1^2 2b_2^2 1b_1^2 5a_1^2 6a_1^1$) show that the cyclic structure has an aromatic two electron π system. The frequencies are 965.9 (b_2,

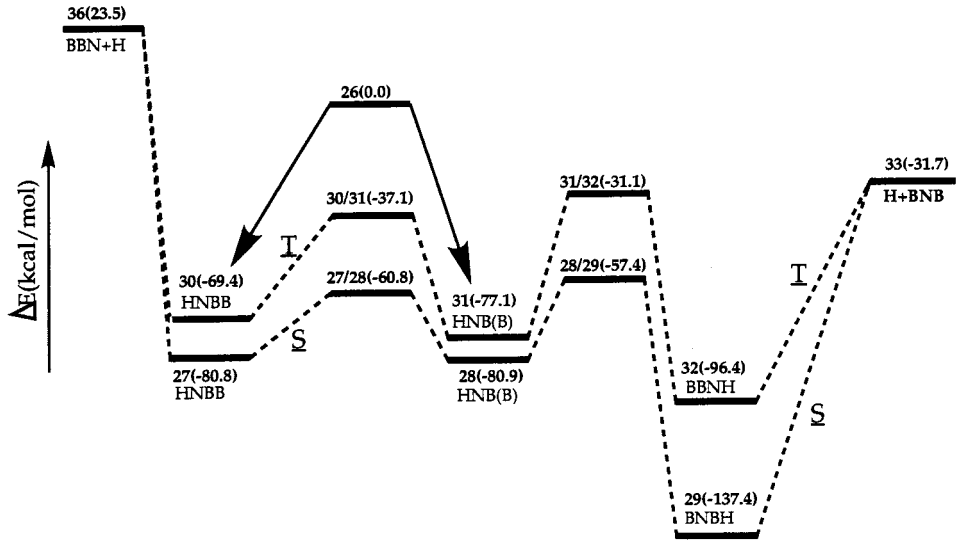

Figure 6. Schematic PES for the reaction B + NH_3 → products. The values in parentheses are the B3LYP/6-311++G(3df,2p) + ZPE (B3LYP/6-31G(d)) relative energies in kcal/mol. T and S represent triplet and singlet, respectively.

TABLE 3: Energies[a] (in kcal/mol) for the Reaction (B + BNH → Products), Together with the B3LYP/6-31G(d) Zero-Point Energies (ZPE, in kcal/mol) and Imaginary Frequencies (IMG, in cm^{-1}) for Transition States

		ZPE[b]	IMG	6-31G(d)	6−311++G(d,p)	6−311++G(2d,p)	6−311++G(3df,2p)[d]
B + HNB	**26**	8.7		0.0 (−104.76702)	0.0 (−104.80754)	0.0 (−104.80979)	0.0 (−104.81345)
					Singlet		
HNBB	**27**	11.0		−81.5	−80.4	−80.3	−80.8
TS	**27/28**	10.3	293.1i	−63.5	−59.7	−60.0	−60.8
BNB(H)	**28**	10.2		−80.6	−79.6	−80.3	−80.9
TS	**28/29**	7.3	1516.7i	−58.1	−55.4	−56.5	−57.4
HBNB	**29**	10.9		−140.3	−135.8	−136.6	−137.4
TS	**29/29**	9.1	1966.8i	−71.8	−67.1	−68.0	−68.3
					Triplet		
BBNH	**30**	11.3		−70.8	−69.0	−68.8	−69.4
TS	**30/31**	10.2	1083.0i	−39.6	−36.3	−36.9	−37.1
BNB(H)	**31**	11.9		−80.3	−75.7	−76.5	−77.1
TS	**31/32**	7.3	1103.0i	−32.6	−29.5	−30.3	−31.1
HBNB	**32**	9.7		−102.1	−95.0	−95.7	−96.4
H + BNB	**33**	4.1		−35.4	−30.2	-−31.0	−31.7
B + HBN	**34**	8.7		33.5	37.5	37.4	37.6
HB + NB	**35**	6.4		96.1	99.7	99.3	99.3
BBN + H	**36**	4.4		17.0	25.6	23.1	23.5
B_2 + NH	**37**	6.0		80.1	87.4	87.6	88.8

[a] Corrected with the B3LYP/6-31G(d) zero-point energies (scaled by a factor of 0.9804[32]). [b] Scaled zero-point energies. [c] Values in parentheses are the total energies in au. [d] Single-point calculations at the B3LYP/6-311++(2d,p) geometries.

82(IR intensity)), 1073.1(a_1, 3), 1471.6(a_1, 11) cm^{-1}, respectively. Scaled by a factor of 0.9613,[32] the frequency (928.5 cm^{-1}) of the asymmetric stretching mode is close to 901.5 cm^{-1} value assigned to cyclic-B_2N experimentally.[8] In addition, we note that the B3LYP/6-31G* harmonic frequencies (scaled by a factor of 0.9613[32]) for linear BNB, 147.9(1), 1149.0 (9), and 1279.4 (4000) cm^{-1}, are significantly different from previously reported UHF/6-31G* values,[18] 82(5), 1245(0), and 2271 (8782) cm^{-1}, respectively.

Comparison with C_3^+. C_3^+ (isoelectronic with BNB) has been studied by several theoretical groups.[41−44] The ground state of C_3^+ has two minima: a cyclic $^2B_2$ state with C_{2v} symmetry is about 5.2 kcal/mol more stable than the linear $^2\Sigma_u^+$ form.[41] Our B3LYP calculations on C_3^+ also found a cyclic C_{2v} structure. Two equal C−C bond distances and the C−C−C bond angle between them were computed to be 1.310 Å and 66.8°, respectively. The previously reported bond distances range from 1.283 to 1.350 Å, and the bond angles range between 67.0° and 73.1°.[41−44] Due to symmetry breaking, we found a $C_{\infty v}$ rather than a $D_{\infty h}$ structure (the two C−C bond distances are 1.241 and 1.342 Å, respectively). Note that the wave function of $D_{\infty h}$ structure, optimized at the HF/6-31G* level, is unstable. Similarly, when the initial guess was altered, we also obtained another bent $^2A_1$ ($4a_1^2 2b_2^2 1b_1^2 5a_1^2 6a_1^1$) C_3^+. In contrast to BNB, this form is only slightly higher in energy (3.6 kcal/mol) than the $^2B_2$ state. The lengths of the equal C−C bonds and the C−C−C bond angles are 1.386 Å and 54.9°, respectively.

B + BNH → Products. BNH is one of the important species generated in the initial reaction. The reaction of BNH (doublet) with a second boron atom B(^2P) may occur on either the singlet or the triplet PES (see Figure 6). The relative energies and geometries are given in Table 3 and in Figure 7, respectively. On the singlet PES, the addition of B to HNB can take place at either the B or the N atom of BNH, resulting in the complexes **27** (BBNH) or **28** (HNB(B)), respectively. Both **27** and **28** are 80.8 kcal/mol below the energy of the B + BNH (**26**) reactants and are linked by a transition state (**27**/**28**) that is 60.8 kcal/mol lower in energy than **26**. Two reactions take place from **28**: direct dissociation into H + BNB (**33**) (which is 31.7 kcal/mol lower than **26**) and rearrangement into **29** (HBNB) via

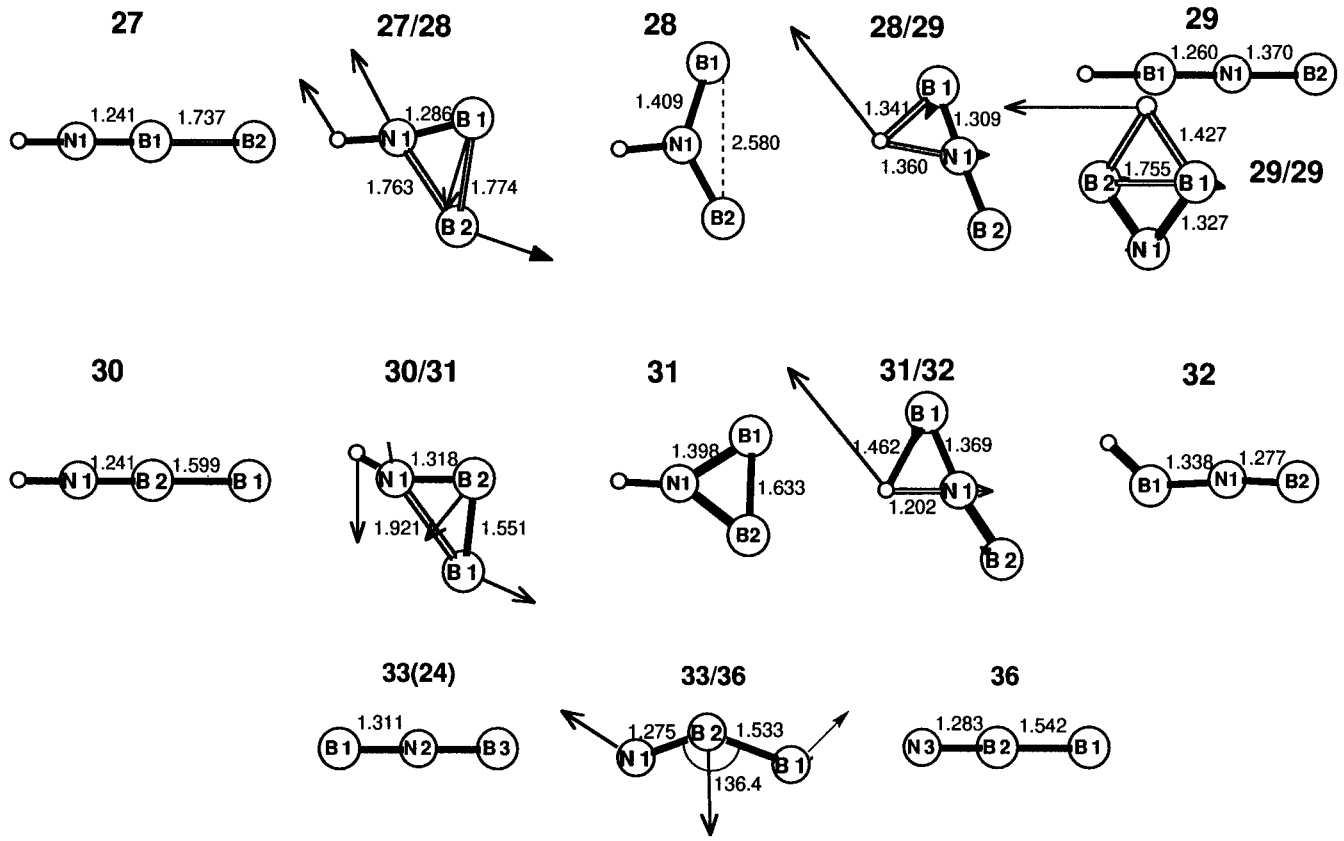

Figure 7. B3LYP/6-311++G(2d,p) structures for the stationary points along the pathway of the reaction B + BNH → products. Bond lengths are given in angstroms and angles in degrees.

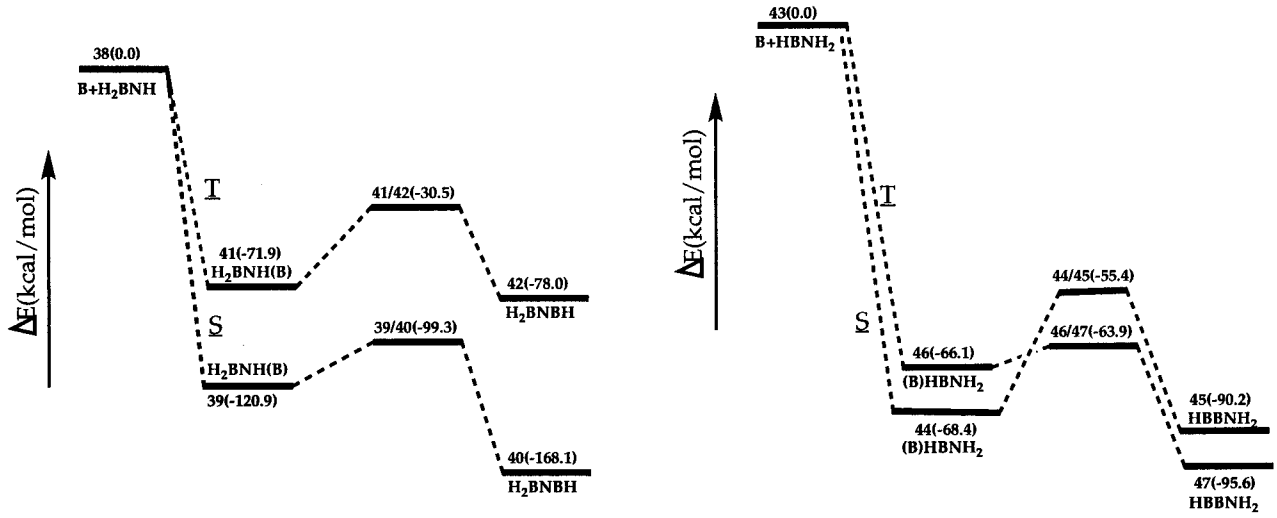

Figure 8. Schematic PES for reactions B + H_2BNH → products (A) and B + $HBNH_2$) → products (B). The values in parantheses are the B3LYP/6-311++G(3df,2p) + ZPE (B3LYP/6-31G(d)) relative energies in kcal/mol. T and S represent triplet and singlet, respectively.

transition state **28/29**. H + BNB (**33**), HBN + B (**34**), and HB + NB (**35**) can be considered to be possible groups of dissociation products from **29.** Among these three possibilities, dissociation into H + BNB (**33**) is the most favorable. Two groups of dissociation products can arise from **27**, B_2 + NH (**36**) and BBN + H (**37**). However, both groups are above the reactants in energy, and the dissociation reactions are unfavorable energetically. HBNB (**29**) is linear, and the energy barrier for H transfer from one end to other via the C_{2v} transition state **29/29** was computed to be 69.1 kcal/mol.

While the reactions on the triplet PES are similar to those on the singlet surface, the energy of the triplet path is the higher and the geometries of the stationary points are different. As on the singlet PES, the most favorable dissociation reaction of the triplet complexes leads to H + BNB (**33**). The linear BNB molecule observed experimentally[7,8] probably arises from the B + BNH reaction.

B + H_2BNH ($HBNH_2$) → Products. Both the H_2BNH (**4**) and $HBNH_2$ (**3**) species, the major products generated initially, can react with a second boron atom either on the singlet or on the triplet PES's. Parts A and B of Figure 8 illustrate schematic pathways for the B + H_2BNH and the B + $HBNH_2$ reactions, respectively; the geometries of the stationary points are displayed in Figure 9.

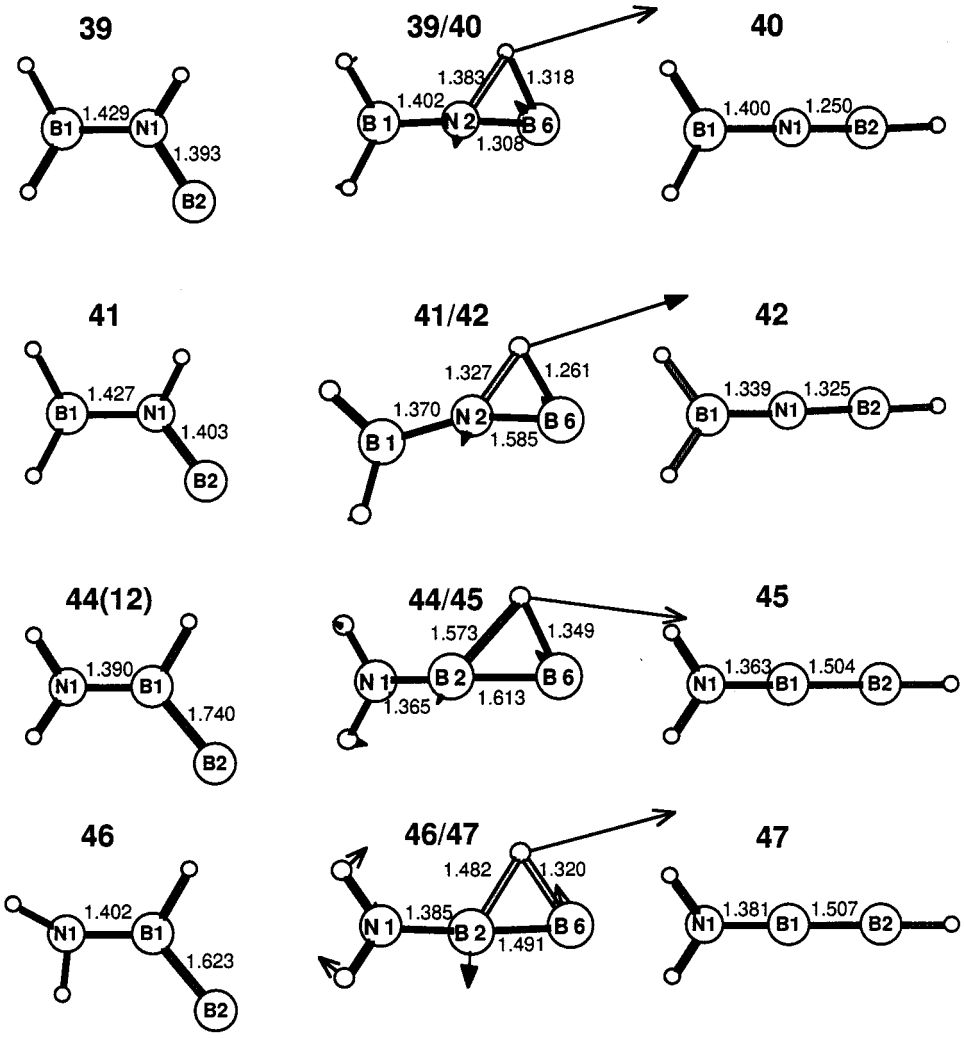

Figure 9. B3LYP/6-311++G(2d,p) structures for the stationary points along the reaction pathways of B with H_2BNH and with $HBNH_2$. Bond lengths are in angstroms.

TABLE 4: Energies[a] (in kcal/mol) for the Reactions B + $BHNH_2$ (H_2BNH) → Products, Together with the B3LYP/6-31G(d) Zero-Point Energies (ZPE, in kcal/mol) and Imaginary Frequencies (IMG, in cm^{-1}) for Transition States

		ZPE[b]	IMG	6−31 G(d)	6−311++G(d,p)	6−311++G(2d,p)	6−311++G(3df,2p)[d]
				B + H_2BNH → H_2BNBH (Singlet)			
B+H_2BNH	38	18.8		0.0 (−106.00804)[c]	0.0 (−106.04684)	0.0 (−106.04926)	0.0 (−106.05316)
H_2BNH(B)	39	23.8		−120.7	−119.8	−120.6	−120.9
TS	39/40	20.7	1408.8i	−100.1	−97.4	−98.6	−99.3
H_2BNBH	40	22.4		−152.9	−164.0	−164.8	−168.1
				B + H_2BNH → H_2BNBH (Triplet)			
H_2BNH(B)	41	24.0		−73.6	−71.2	−71.7	−71.9
TS	41/42	20.7	2110.6i	−33.3	−29.0	−29.9	−30.5
H_2BNBH	42	20.6		−64.5	−77.8	−78.3	−78.0
				B + $HBNH_2$ → $HBBNH_2$ (Singlet)			
B+$HBNH_2$	43	22.4		0.0 (−106.01428)	0.0 (−106.05856)	0.0 (−106.06063)	0.0 (−106.06441)
(B)$HBNH_2$	44	24.7		−68.5	−68.1	−68.3	−68.4
TS	44/45	22.2	845.5i	−53.7	−54.7	−54.9	−55.4
$HBBNH_2$	45	24.5		−89.1	−89.9	−89.7	−90.2
				B + $HBNH_2$ → $HBBNH_2$ (Triplet)			
(B)$HBNH_2$	46	24.7		−67.8	−65.5	−65.7	−66.1
TS	46/47	22.2	337.9i	−63.1	−62.9	−63.3	−63.9
$HBBNH_2$	47	23.7		−95.8	−95.3	−95.1	−95.6

[a] Corrected with the B3LYP/6-31G(d) zero point energies (scaled by a factor of 0.9804[32]). [b] Scaled zero point energies. [c] Values in parenthe and Imaginary Frequencies (IMG, in cm^{-1}) for Transition States.ses are the total energies in au. [d] Single point calculations at the B3LYP/6-311++(2d,p) geometries.

The B reacts with H_2BNH on the singlet PES via initial formation of a complex (**39**) followed by an H migration transition state **39/40**. The energies of the intermediate complex, the transition state, and the product relative to the reactants (**38**) are −120.9, −99.3, and −168.1 kcal/mol, respectively. Andrews et al.[7] observed the H_2BNBH product **40** in their matrix isolation

study. The B + H_2BNH reaction on the triplet PES has a similar mechanism to that on the singlet PES (details are given in Figure 8A and Table 4).

The basic path for the reaction of a B atom with $HBNH_2$ (Figure 8B) is quite similar to the reaction of B with H_2BNH (Figure 8A). Energetic and geometric data related to the B + $HBNH_2$ reaction are given in Table 4.

Conclusions

The initial stage of the reaction of a boron atom with ammonia involves insertion into a N−H bond. An intermediate complex (BNH_3) is formed followed by H-migration to give $HBNH_2$. This insertion mechanism resembles the B insertion into H_2O but differs from the B insertion into CH_4 (which does not involve an intermediate complex). Several species such as H_2BNH, HBNH, and BNH are generated from $HBNH_2$ by rearrangement and dissociation. A second boron atom can react with the species to give novel species such as HBNBH, BNB, BNBH, H_2BNBH, etc. Unlike the isoelectronic C_3^+, which has both a bent and a linear minimum close in energy, the isoelectronic BNB has a linear ground state ($^2\Sigma_u^+$) and only a high-energy $^2A_1$ cyclic-B_2N form.

The B_2−ammonia insertion mechanism resembles that for a single boron atom, but B_2 is much more reactive. This is consistent with the earlier results for the B_2 and B insertions into CH_4 and H_2O.

Acknowledgment. The National Natural Science Foundation Committee of China provided financial support. We also thank Dr. J. M. L. Martin for discussions on the structure of B_2N, as well as Prof. L. Andrews and Prof. O. Charkin for their interest.

References and Notes

(1) Hannachi, Y.; Hassanzadeh, P.; Andrews, L. *J. Phys. Chem.* **1994**, *98*, 6950.
(2) Hassanzadeh, P.; Hannachi, Y.; Andrews, L. *J. Phys. Chem*. **1993**, *97*, 6418.
(3) Jeong, G. H.; Boucher, R.; Klabunde, K. J. *J. Am. Chem. Soc*. **1990**, *112*, 3332.
(4) Wang, Z.-X.; Huang, M.-B. *J. Am. Chem. Soc*. **1998**, *120*, 6758.
(5) Lebrilla, C. B.; Maier, W. F. *Chem. Phys. Lett*. **1984**, *105*, 183.
(6) Hassanzadeh, P.; Andrews, L. *J. Am. Chem. Soc*. **1992**, *114*, 9239.
(7) Thompson, C. A.; Andrews, L. *J. Am. Chem. Soc.* **1995**, *117*, 10125.
(8) (a) Thompson, C. A.; Andrews, L.; Martin, J. M. L.; El-Yazel, J. *J. Phys. Chem.* **1995**, *99*, 13839. (b) Andrews, L. Private communication.
(9) Knight, L. B., Jr.; Herlong, J. O.; Kirk, T. J.; Arrington, C. A. *J. Chem. Phys.* **1992**, *96*, 5604.
(10) Knight, L. B.; Hill, D. W.; Kirk, T. J.; Arrington, C. A. *J. Phys. Chem*. **1992**, *96*, 555.
(11) . Andrews, L.; Burkholder, T. R. *J. Phys. Chem*. **1991**, *95*, 8554.
(12) Sakai, S.; Jordan, K. D. *J. Phys. Chem*. **1983**, *87*, 2293.
(13) Martin, J. M. L.; Taylor, P. R.; Hassanzadeh, P.; Andrews, L. *J. Am. Chem. Soc*. **1993**, *115*, 2510.
(14) Andrews, L.; Hassanzadeh, P.; Martin, J. M. L.; Taylor, P. R. *J. Phys. Chem.* **1993**, *97*, 5839.
(15) Flores, J. R.; Largo, A. *J. Phys. Chem.* **1992**, *96*, 3015.
(16) Sakai, S.; Morokuma, K. *J. Phys. Chem.* **1987**, *91*, 1.
(17) Martin, J. M. L.; Francois, J. P.; Gijbels, R. *J. Chem. Phys.* **1989**, *90*, 6469.
(18) (a) Hassanzadeh, P.; Andrews, L. *J. Phys. Chem*. **1992**, *96*, 9177.
(19) Andrews, L.; Hassanzadeh, P.; Burkholder, T. R.; Martin, J. M. L. *J. Chem. Phys*. **1993**, *98*, 922.
(20) Burkholder, T. R.; Andrews, L.; Bartlett, R. J. *J. Phys. Chem*. **1993**, *97*, 3500.
(21) Burkholder, T. R.; Andrews, L. *J. Phys. Chem*. **1992**, *96*, 10195.
(22) Hamrick, Y. M.; Van Zee, R. J.; Godbout, J. T.; Weltner, W., Jr.; Lauderadle, W. J.; Santon, J. F.; Bartlett, R. J. *J. Phys. Chem.* **1991**, *95*, 2840.
(23) Burkholder, T. R.; Andrews, L. *J. Chem. Phys*. **1991**, *95*, 8697.
(24) Tague, T. J., Jr.; Andrews, L. *J. Am. Chem. Soc.* **1994**, *116*, 4970.
(25) (a) Lory, E.; Porter, R. *J. Am. Chem. Soc*. **1973**, *95*, 1767. (b) Kawashima, Y.; Kawaguchi, K.; Hirota, E. *J. Chem. Phys.* **1987**, *87*, 6331. (c) Dill, J. D.; Schleyer, P. v. R.; Pople, J. A. *J. Am. Chem. Soc*. **1975**, *97*, 3402. (d) Summers, N.; Tyrell, J. *J. Am. Chem. Soc.* **1977**, *99*, 3960. (e) DeFrees, D. J.; Binkley, J. S.; McLean, A. D. *J. Chem. Phys.* **1984**, *80*, 3720.
(26) (a) Paetzold, P. *Pure Appl. Chem*. **1991**, *63*, 345. (b) *Adv. Inorg. Chem*. **1993**, *32*, 3755.
(27) Kuhn, H. G. *Atomic Spectra*; Academic Press: New York, 1962.
(28) Huber, K. P.; Herzberg, G. *Molecular Spectra and Molecular Structure. IV. Constants of diatomic molecules*; Van Nostrand Reinhold Company: New York, 1979.
(29) Becke, A. D. *J. Chem. Phys.* **1993**, *98*, 5648. (b) Lee, C.; Yang, W.; Parr, R. G. *Phys Rev. B* **1988**, *37*, 785.
(30) Frisch, M. J.; Trucks, G. W.; Schlegel, H. B.; Gill, P. M. W.; Johnson, B. G.; Robb, M. A.; Cheeseman, J. R.; Keith, T.; Petersson, G. A.; Montgomery, J. A.; Raghavachari, K.; Al-Laham, M. A.; Zakrzewski, V. G.; Ortiz, J. V.; Foresman, J. B.; Cioslowski, J.; Stefanov, B. B.; Nanayakkara, A.; Challacombe, M.; Peng, C. Y.; Ayala, P. Y.; Chen, W.; Wong, M. W.; Andres, J. L.; Replogle, E. S.; Gomperts, R.; Martin, R. L.; Fox, D. J.; Binkley, J. S.; Defrees, D. J.; Baker, J.; Stewart, J. P.; Head-Gordon, M.; Gonzalez, C.; Pople, J. A. *Gaussian 94*; Gaussian, Inc.: Pittsburgh, PA, 1995.
(31) Hehre, W. J.; Random, L.; Schleyer, P. v. R.; Pople, J. A. *Ab Initio Molecular Orbital Theory*; Wiley: New York, 1986.
(32) Foresman, J. B.; Frisch, A. *Exploring Chemistry with Electronic Structure Method*, 2nd ed.; Gaussian, Inc.: Pittsburgh, PA, 1995 and references therein.
(33) Curtiss, L. A.; Raghavachari, K.; Trucks, G. W.; Pople, J. A. *J. Chem. Phys*. **1991**, *94*, 7221.
(34) (a) Cizek, J. *Adv. Chem. Phys*. **1969**, *14*, 35. (b) Purvis, G. D.; Bartlett, R. J. *J. Chem. Phys*. **1982**, *76*, 1910. (c) Scuseria, G. E.; Janssen, C. L.; Schaefer, H. F., III *J. Chem. Phys*. **1988**, *89*, 7382. (d) Scuseria, G. E.; Schaefer, H. F., III *J. Chem. Phys.* **1989**, *90*, 3700. (e) Pople, J. A.; Head-Gordon, M.; Raghavachari, K. *J. Chem. Phys*. **1987**, *87*, 5968.
(35) Wang, Z.-X.; Liu, R.-Z.; Huang, M.-B.; Yu, Z. *Can. J. Chem*. **1996**, *74*, 910.
(36) Wang, Z.-X.; Huang, M.-B.; Liu, R.-Z. *Can. J. Chem*. **1997**, *75*, 996.
(37) Wang, Z.-X.; Huang, M.-B. *J. Phys. Chem*. A **1998**, *102*, 229.
(38) Wang, Z.-X.; Huang, M.-B. *J. Chem. Soc., Faraday Trans*. **1998**, *94*, 635.
(39) Sakai, S. *J. Phys. Chem*. **1992**, *96*, 8369.
(40) Martin, J. M. L. Private communication.
(41) Taylor, P. R.; Martin, J. M. L.; Francois, J. P.; Gijbels, R. *J. Phys. Chem*. **1991**, *95*, 6530.
(42) Grev, R. S.; Alberts, I. L.; Schafer, H. F. *J. Phys. Chem.* **1990**, *94*, 3379.
(43) Raghavachari, K. *Chem. Phys. Lett*. **1990**, *171*, 249.
(44) Martin, J. M. L.; Francois, J. P.; Gijbels, R. *J. Chem. Phys*. **1990**, *93*, 5307.